Picosatellite identification and Doppler estimation using passive radar techniques

Tibor Herman and Levente Dudás

Abstract—In this article a novel method for satellite identification is presented for picosatellites. Utilizing apriori knowledge of the transmitted signals the cross-correlation of the received signal and a known transmission is calculated, from the results the Doppler shift is estimated and the satellite's Doppler curve can be matched against the measurements of NORAD. Using this method an omnidirectional antenna can be used instead of a high gain directional antenna, and the gain difference is compensated by the processing gain of the algorithm described. The practicality of the algorithm is demonstrated through the mission of MRC-100 PocketQube.

Index Terms—PocketQube, satellite identification, remote sens- ing, signal processing, passive radar

I. INTRODUCTION

SINCE 2021 the popularity of the picosatellite category called PocketQube has been rising rapidly, with a growing number of them being deployed [1]–[5]. They are usually put to orbit in groups, which means that the small distance between them and their radar cross section makes the individual identification by ground based radar systems challenging. The base unit of such spacecraft is a 5 cm cube, which is close to the minimum detection size of the North American Aerospace Defense Command's (NORAD) radars [6]. Especially at the beginning of a mission the two-line element set (TLE) provided by them can be quite inaccurate, because they are not updated every day and there are several unidentified sets that correspond to the targets close to each other. This, in conclusion degrades the reception quality of the ground stations, because the Doppler estimation relies on these measurements.

Since the available onboard power of a PocketQube is limited, the transmission power is usually in the range of 100 mW or 20 dBm. It produces a received power level on the ground station that has little margin in the link budget, so usually the tracking of such satellites is done using directional antennas, which have to track the movement of the spacecraft. The accuracy of tracking is mainly defined by the available TLE provided by NORAD [8].

The aim of this paper is to provide a means for identifying pico satellites without an expensive tracking and antenna system, using a simple omnidirectional antenna, such as a ground plane or dipole. The gain lost due to the lack of tracking and antenna gain is recovered by the processing gain introduced during signal processing. In the following sections,

T. Herman and L. Dudás are with Budapest University of Technology and Economics, Department of Broadband Infocommunications and Electromagnetic Theory, Faculty of Electrical Engineering and Informatics, Budapest, Hungary. (e-mail: herman.tibor@vik.bme.hu, dudas.levente@vik.bme.hu)

the latest satellite mission of the university will be used to demonstrate the practicality of the algorithm described.

There have been little research on the topic, the most relevant paper in this field detects the reflected signal of GRAVES (French: Grand Réseau Adapté à la Veille Spatiale), which is a French radar surveillance system, transmitting on 143,05 MHz [9]. In this paper the authors were able to detect satellites on low Earth orbit in the range of several hundred kilograms.

In [10], [11] the authors use the forward scattered signals of a broadcast satellite to detect high altitude targets, like a space shuttle and they emphasize the importance of the large radar cross-section (RCS) required for this technique to work. A picosatellite, like a PocketQube has much smaller RCS, so although it seems possible, research has to be done to find out about the feasibility regarding small targets.

To increase the quality of reception we propose an algorithm that measures the Doppler shift of the received signal by cross-correlating the received samples with a predefined pattern that is transmitted periodically by the on board radio. This method is usually used in passive radar applications, where a radio receiver is used to measure the distance and relative velocity of a target without transmitting anything. It relies on ambient signals that are transmitted by high power broadcast stations. The reference signal received by the observer is compared with its Doppler shifted and time delayed copies to produce a correlation peak in the ambiguity function [12], [13].

MRC-100 (Fig. 1) is a 3 unit PocketQube satellite developed by students and lecturers of Technical University of Budapest. It was named after Műegyetemi Rádió Club, honoring its 100th anniversary in 2024. It is the latest member of the SMOG satellites, whose task is to monitor human caused electromagnetic pollution on a low Earth orbit [15], [16]. The satellite transmits packets periodically on 436.72 MHz using Gaussian Minimum Shift Keying (GMSK) modulation [8]. Non-coherent synchronization bits found in the packets are used as a reference signal which are compared against the incoming signal, while the incoming signal is delayed and shifted in frequency. The output of the correlation function has a global maximum where the two signals match in the delay-Doppler matrix, assuming that the signal we are looking for is present in the received signal.

II. SIGNAL DETECTION

To detect a predefined signal in a received noisy signal that is shifted due to the Doppler effect, the 2D cross-correlation function of the two signals have to be calculated while one of the signals is copied with Doppler shift. Its discrete time
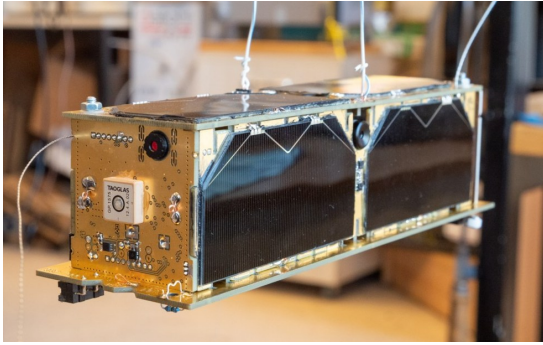
Picosatellite identification and Doppler estimation
using passive radar techniques

Fig. 1. MRC-100 flight model

definition is given by Eq. 1, where n is the sample delay, f_D is the Doppler shift, $r(k - \frac{n}{2})$ is the received signal and $x^*(k + \frac{n}{2})$ is the complex conjugate of the signal pattern we are looking for in the n, f_d domain [12]. The procedure is done on blocks of signals, which have N samples. Eq. 2 is a simplified version, where y is the conjugate of x multiplied by the rotational vector. If a distinct correlation peak is found in the function output, it means that the pattern matches the incoming signal with the given frequency shift and time delay. Over time, if the received signal contains the packets, the correlation peaks follow a tangent-function.

$$R(n, f_d) = \sum_{k=-N}^{N-1} r\left(k - \frac{n}{2}\right) \cdot x^*\left(k + \frac{n}{2}\right) e^{j 2\pi f_d \frac{k}{N}} \quad (1)$$

$$R(n, f_d) = \sum_{k=-N}^{N-1} r\left(k - \frac{n}{2}\right) \cdot y\left(k + \frac{n}{2}, f_d\right) \quad (2)$$

Eq. 2 is a convolution, but one of the signals is reversed in time. Using the convolution theorem, we know that the product of the Fourier-transform of two signals is equal to the convolution of the two signals (Eq. 3). If we take the inverse Fourier-transform of the product (Eq. 4), we get the cross-correlation of the two signals [14].

$$\mathcal{F}\{R(n, f_d)\} = \mathcal{F}\left\{r\left(k - \frac{n}{2}\right)\right\} \cdot \mathcal{F}^*\left\{y\left(k + \frac{n}{2}, f_d\right)\right\} \quad (3)$$

$$R(\tau, f_d) = \mathcal{F}^{-1}\left[\mathcal{F}\left\{r\left(t - \frac{\tau}{2}\right)\right\} \cdot \mathcal{F}^*\left\{y\left(t + \frac{\tau}{2}, f_d\right)\right\}\right] \quad (4)$$

Since the signal processing is done on discrete time sampled signals, discrete Fourier-transform, more specifically Fast Fourier Transform (FFT) is used for better computation efficiency. To shift a signal in the frequency domain (to apply Doppler shift) the FFT of the signal is shifted circularly.

Fig. 2 shows the operations that are carried out periodically on the incoming signal. First, the reference signal is moved to frequency domain by FFT, which is shifted circularly so the frequency shifted copies of the signal without excessive computations are obtained. The incoming complex samples are moved to frequency domain by FFT, then the complex conjugate of the signal is multiplied by each frequency shifted

copy of the reference signal. After a two dimensional inverse FFT (IFFT) we get the double-sided delay-Doppler function.
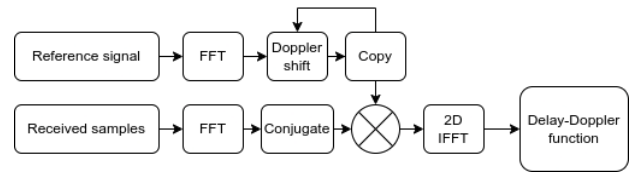

Fig. 2. The signal processing chain

The output of the correlator is processed in blocks, whose size is determined by the length of the reference signal and the desired Doppler range. The complex float output is converted to absolute values on a logarithmic scale, then after a maximum search algorithm, the values are converted to a bitmap file. Lastly, the images are merged together into a montage, which yields the delay-Doppler image for the observed samples in blocks.

Fig. 3 shows the correlation peak at the center which represents the 0 delay and 0 Hz Doppler shift. As the incoming packets arrive at random times, the correlation peak moves left and right based on the sample delay and moves up and down according to the Doppler frequency. The length of the reference signal determines the correlation length and the maximum delay the function is able to show. On the vertical axis the range of Doppler shift is set manually, based on the maximum observable shift of the signal of the target satellite. In the case of Low Earth Orbit (LEO) satellite orbiting at 500 km above Earth the first orbital speed is defined as

$$v = \sqrt{\frac{Gm_E}{r}} = $$
$$= \sqrt{\frac{6.673 \cdot 10^{-11} \frac{Nm^2}{kg^2} \cdot 5.9 \cdot 10^{24} kg}{6370000m + 500000m}} = 7615 \frac{m}{s} \quad (5)$$

where G is the the gravitational constant of Earth, m_E is the mass of Earth and r is the distance of the object from the center of the Earth. Using the velocity of the satellite and assuming a stationary receiver, we can calculate maximum observable Doppler frequency using Eq. 6, where f_0 is the transmitter frequency, c is the speed of light and v_t is the transmitter velocity.

$$f_D = \left|f_0 - f_0 \frac{c}{c + v_t}\right| = 11085 Hz \quad (6)$$

The resolution of the Doppler frequency estimation depends on the sampling rate (f_s) and the length of the FFT (N), the exact value is $\frac{f_s}{N}$.

III. The communication subsystem of MRC-100

Nowadays, small satellites use low cost, single chip radio transceivers to transfer data between the satellite and their ground station. Most of these use digital frequency modulation or frequency shift keying (FSK) for which a non-coherent receiver structure can be used. Therefore, bit and frame synchronization is done on a packet basis, using a preamble (usually 0101 sequences) and a sync word that has
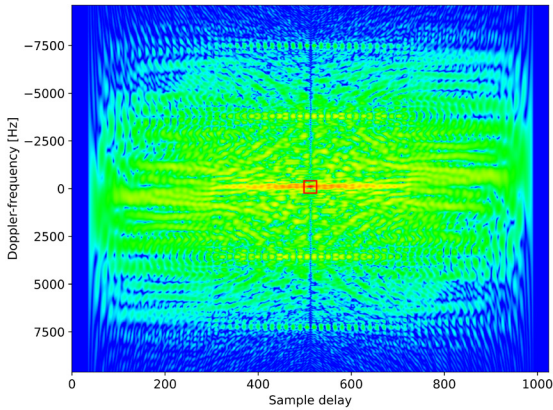
Fig. 3. The delay-Doppler function with simulated signal, $0\,\mathrm{dB}$ SNR and $0\,\mathrm{Hz}$ Doppler

good auto-correlation properties. In the case of MRC-100 the communication subsystem (Fig. 4) uses an Acsip S68F integrated radio which is capable of handling LoRa and FSK transmissions (Fig. 6). It contains an SX1268 silicon along with a matching network that transforms the input/output impedance to $50\,\Omega$ and an integrated temperature compensated crystal oscillator (TCXO) as the reference clock.

As an essential component of the satellite, the communication module is designed to withstand single point failures by incorporating cold redundancy. Figure 5 shows how the two radios share the same antenna: we use radio frequency PIN (Positive Intrinsic Negative) diodes to connect them one at a time. In order to prevent over-current or overvoltage events, each radio is equipped with a dedicated limiter switch that automatically shuts off.

Telemetry packets use GMSK modulation and have a 32 bit standard 0101 preamble and a 32 bit sync word which is 0xE31C9DAE. This sequence is transmitted at the beginning of every single packet, so searching for this portion of data in the incoming signal regardless of the useful data in the packet produces cross-correlation peaks at the actual Doppler frequency.

Fig. 4. The UHF communication subsystem of MRC-100

Fig. 5. The block diagram of the UHF communication subsystem of MRC-100

IV. MRC-100 TELEMETRY PROPERTIES

The mathematical formula of general frequency modulated (FM) signal is defined as

$$s_{FM}(t) = V_c cos\left(\omega_c t + 2\pi k_{FM}\int_0^t s_m(\tau)d\tau\right) \quad (7)$$

If we consider a sinusoidal modulating signal, $s_m(t) = V_m cos(\omega_m t)$ then the after integration Eq. 7 becomes

$$s_{FM}(t) = V_c cos\left(\omega_c t + 2\pi k_{FM}V_m\frac{sin(\omega_m t)}{\omega_m}\right) \quad (8)$$

Substituting ω_m by $2\pi f_m$ and defining $f_d = k_{FM}V_m$ as frequency deviation we get

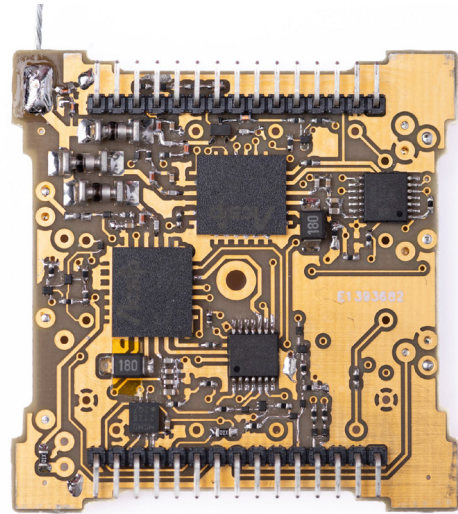$$s_{FM}(t) = V_c cos\left(\omega_c t + 2\pi f_d\frac{sin(2\pi f_m t)}{2\pi f_m t}\right) \quad (9)$$
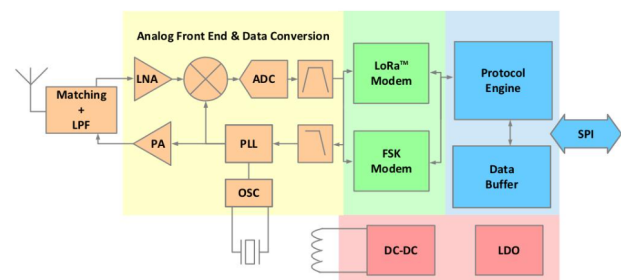

Fig. 6. The block diagram of the Semtech SX1268 radio [7]

after simplification the the equation for an FM signal with sinusoidal modulating signal becomes

$$s_{FM}(t) = V_c cos\left(\omega_c t + \frac{f_d}{f_m} sin(2\pi f_m t)\right) \qquad (10)$$

If the modulating signal is a digital square wave, we get the resultant FSK signal (Eq. 11) by substituting the function of the sequence into Eq. 7, where E_b is the bit energy, T_b is the bit time, $\omega_c = 2\pi f_c$ is the carrier angular frequency, k_{FM} is the modulation index, $d_k \in -1, +1$ is the data bit sequence and P_{Tb} is the impulse function. If the data rate is

$$s_{FSK}(t) =$$
$$\sqrt{\frac{E_b}{T_b}} cos\left(\omega_c t + 2\pi k_{FM} \int_0^t \sum_{k=0}^{N-1} d_k P_{Tb}(\tau - kT_b)d\tau\right)$$
$$(11)$$

MRC-100 transmits telemetry packet groups (Fig. 7) periodically in normal operation. The period of the cycle is about 15 seconds and the default telemetry contains a LoRa (Long Range) modulated identification beacon, six GMSK telemetry packets and a synchronization packet. Each type has a different data rate: the synchronization packet is always transmitted at 5 kbps, the telemetry packets can be configured by ground station commands and their data rate is 12.5 kbps in normal operation. The LoRa beacon is also configurable, the default settings use SF12 with 12.5 kHz bandwidth with and air time of 892 ms [8].
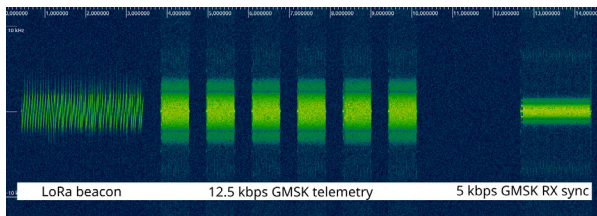
Fig. 7. The default telemetry packets of MRC-100

A. GMSK synchronization packet

MRC-100 uses a synchronization packet using GMSK modulation parameters and fixed data content that which is a pseudo random bit sequence (PRBS) sequence that helps the ground station schedule the telecommand packets.

By analyzing the the auto-correlation function of the packet, a peak that excels 12 dB from the noise floor can be seen (Fig. 8), meaning that a processing gain of 12 dB can be achieved. This makes detection possible even with a simple, stationary omnidirectional antenna with low gain, instead of using a directional antenna.

V. SIMULATION RESULTS

The performance of the algorithm was evaluated using simulated signals. The time-domain samples of the frequency sync and frame sync bits are resampled, a square signal of +1 and -1 values are generated and filtered with a Gaussian window (BT=0.5) Finite Impulse Response (FIR) filter, which
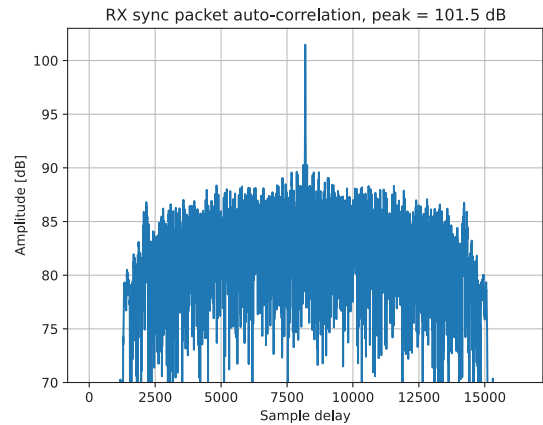
Fig. 8. The normalized auto-correlation function of the RX sync packet

are then frequency modulated and multiplied by a carrier signal as shown in Fig. 9. The intermediate signals and the spectrum of the generated signal are shown in Fig. 10.
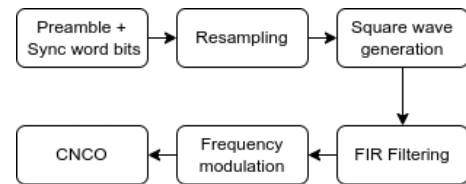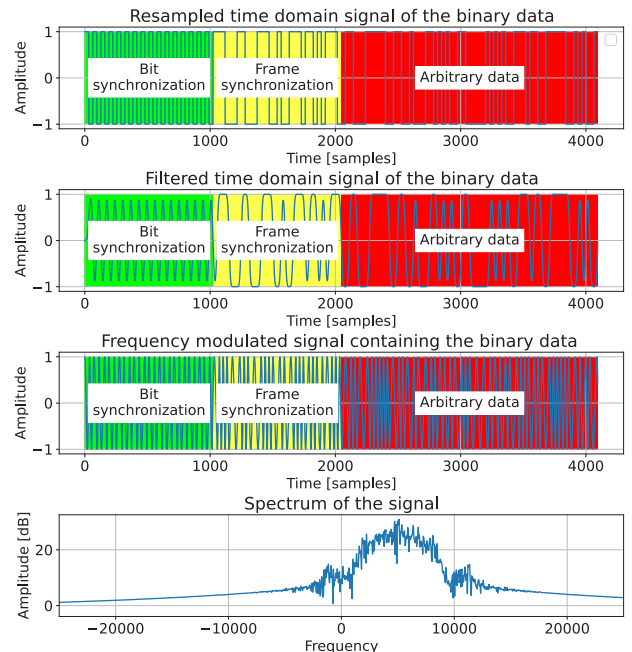
Fig. 9. Flowchart of the GMSK signal simulation

Fig. 10. Simulation of the GMSK modulated packet with highlighted bit sync and frame sync

The auto-correlation function of the simulated bit- and
frame sync shown in Fig. 11 provides a 11 dB peak compared
to the sidelobes, although the close vicinity of the peak is
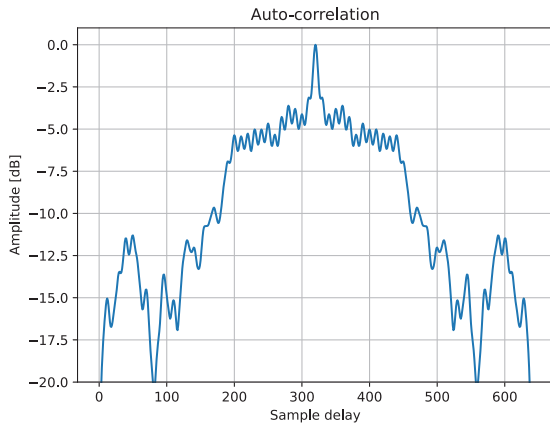around 5 dB, due to the repeating 01 pattern.

Fig. 11.   The normalized auto-correlation function of the bit and frame sync

For the input a list of Doppler frequencies were calculated
using predict, which is an open-source software used for
tracking satellites and celestial bodies [17]. We used the
output to iteratively shift the generated signal in the frequency-
domain so that it can be fed back to the Doppler estimator
input.

A. Results using the bit- and frame sync samples as reference

Figures 12 and 13 show the delay-Doppler function for a
satellite pass where the received signal to noise ratio (SNR)
is 0 dB and -15 dB, respectively. Both results show distinct
peaks that correspond with the Doppler shift of the input.
The simulation outputs the measured frequency shift of the
correlator output's maximum which was compared to the input
values. Figure 14 shows the frequency error of the estimation.
It should be noted that in the simulation the FFT bin size is
$\frac{f_s}{n} = \frac{25000 Hz}{1024} = 24.41 Hz$ so the error range stayed within
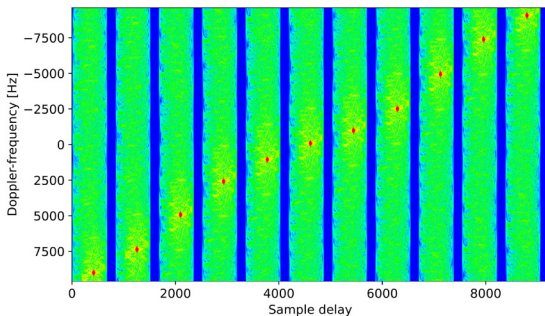one FFT bin at every measurement point.

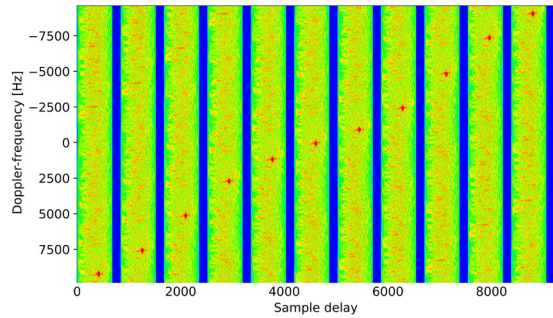Fig. 12.   Doppler estimation for a simulated satellite pass with 0 dB SNR

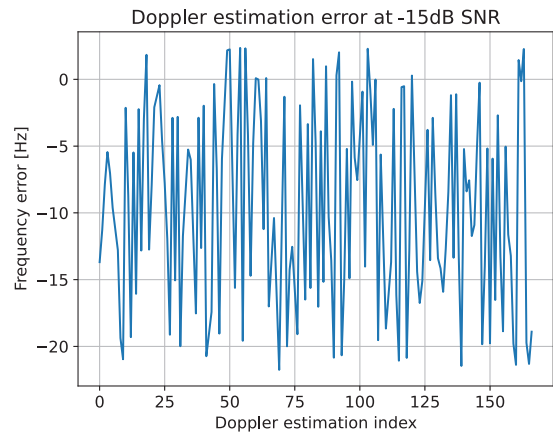Fig. 13.   Doppler estimation for a simulated satellite pass with -15 dB SNR

Fig. 14.   Error of Doppler estimation with -15 dB SNR

B. Results using the synchronization packet

We also evaluated the algorithm using a collection of real-
life samples recorded with a software defined radio (SDR)
with zero Doppler shift. In this recording a variety of signals
(Fig. 15) are present along with four RX synchronization
packets ($2^{nd}, 4^{th}, 5^{th}$ and the last), to observe the behaviour
of the algorithm. In this case the reference signal is longer,
contains more energy so the correlation peak is narrower and
more emphasized compared to the previous case where only
the frame and bit synchronization was used as the reference
signal. The correlator outputs the amplitude of the peak, which
is proportional with the energy of the output signal according
to Eq. 4 . This property of the correlator can be used to
filter false detections. The amplitude threshold of the filter
can be set by observing the distribution of estimated Doppler
– correlation peak amplitude measurements. In Fig. 16 red
and yellow markers show the valid and invalid measurement
points which are classified by their correlation amplitude,
shown in Fig. 17 where correlation peak value is displayed
on a logarithmic scale. Yellow peaks typically have a larger
amplitude than the red ones, indicating a possible detection
of RX synchronization packet in the incoming signal. The
point that shows about -300 Hz Doppler shift indicates a
telecommand packet that was transmitted by the nearby ground
station.

Picosatellite identification and Doppler estimation
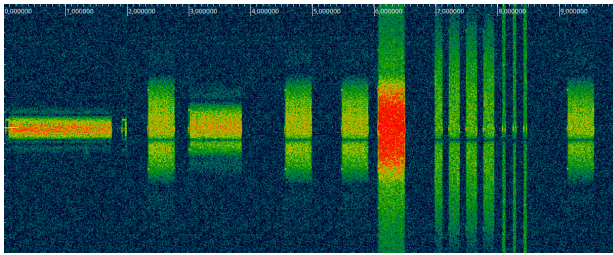using passive radar techniques

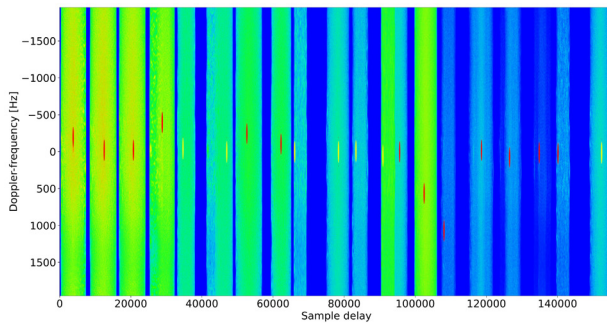Fig. 15. Waterfall spectrum of several packets used for evaluation

Fig. 16. Delay-Doppler estimation of several packets used for evaluation
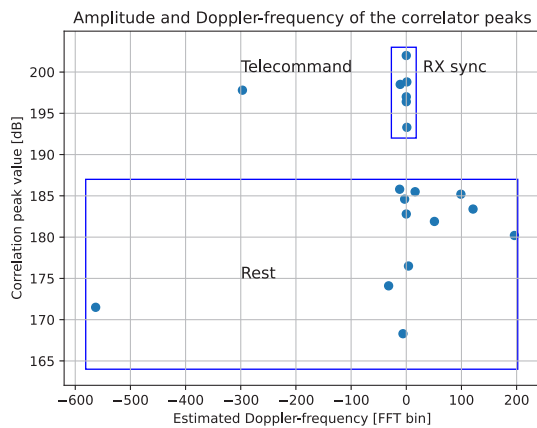

Fig. 17. The amplitude and Doppler shift of correlator peaks

The two results described above show that using the algorithm can be used to estimate the Doppler frequency of the incoming signal if the reference signal is present. However, the measurement output needs to be filtered, since the incoming signal does not always contain the pattern, so based on the amplitude of the correlator peaks, the invalid estimations can be discarded. Running the algorithm on a complete satellite pass can plot the Doppler curve of the orbit, which can be compared with the TLE used for tracking. This can be done with different TLEs that are candidates for the target satellite and the optimal TLE can be selected for future pass(es).

VI. CONCLUSION

The work presented here described how Doppler estimation can be done using little information about the radio transmission parameters of a satellite that is too small to have a precise and up-to-date TLE, especially right after launch, when picosatellites are orbiting in a group with little distance to one another. Using cross-correlation and further signal processing, the Doppler frequency of the transmitted packets were estimated and invalid results were filtered, so an improved curve estimation can be done.

MRC-100 will be delivered to orbit with Transporter-8 Sun-Synchronous Orbit (SSO) Rideshare on 12 June, 2023. According to the launch broker, the two stage deployment will put the satellite 7-14 days after the rocket launch. After a successful beginning of the mission validation measurements will be carried out on actual signals received from the satellite.

REFERENCES

[1] Completed missions of Alba Orbital http://www.albaorbital.com/completed-missions Accessed October 25, 2023

[2] Unisat-7 launch campaign of GAUSS SRL https://www.gaussteam.com/satellites/gauss-latest-satellites/unisat-7/ Accessed October 25, 2023

[3] Firefly's first mission, "To The Black" https://fireflyspace.com/missions/flta002-to-the-black/ Accessed October 25, 2023

[4] Payloads of Transporter-3 mission https://www.eoportal.org/other-space-activities/transporter-3#payloads Accessed October 25, 2023

[5] Payloads of Transporter-5 mission https://www.eoportal.org/other-space-activities/transporter-5#passenger-payloads Accessed October 25, 2023

[6] Speretta, Stefano & Sundaramoorthy, Prem & Gill, Eberhard. (2017). "Long-term performance analysis of NORAD Two-Line Elements for CubeSats and PocketQubes.", *11th IAA Symposium on Small Satellites for Earth Observation,* Berlin, Germany

[7] Datasheet of Semtech SX1268 https://www.semtech.com/products/wireless-rf/lora-connect/sx1268# documentation Accessed October 25, 2023

[8] T. Herman and L. Dudás, "Satellite identification beacon system for PocketQube mission," *2022 24th International Microwave and Radar Conference (MIKON)*, Gdansk, Poland, 2022, pp. 1–5, **DOI**: 10.23919/MIKON54314.2022.9924648.

[9] D. Mieczkowska et al., "Detection of objects on LEO using signals of opportunity," *2017 Signal Processing Symposium (SPSympo)*, Jachranka, Poland, 2017, pp. 1–6, **DOI**: 10.1109/SPS.2017.8053660.

[10] M. Radmard, S. Bayat, A. Farina, S. Hajsadeghian and M. M. Nayebi, "Satellite-based forward scatter passive radar," *2016 17th International Radar Symposium (IRS)*, Krakow, Poland, 2016, pp. 1–4, **DOI**: 10.1109/IRS.2016.7497275.

[11] V. I. Veremyev, E. N. Vorobev and Y. V. Kokorina, "Feasibility Study of Air Target Detection by Passive Radar Using Satellite-based Trans-mitters," *2019 IEEE Conference of Russian Young Researchers in Electrical and Electronic Engineering (EIConRus)*, Saint Petersburg and Moscow, Russia, 2019, pp. 154–157,
DOI: 10.1109/EIConRus.2019.8656630.

[12] T. Pető, L. Dudás and R. Seller, "DVB-T based passive radar," *2014 24th International Conference Radioelektronika*, Bratislava, Slovakia, 2014, pp. 1–4, https://doi.org/10.1109/Radioelek.2014.6828433.

[13] T. Pető, "Multichannel passive radar receiver platform," *2015 17th International Conference on Transparent Optical Networks (ICTON)*, Budapest, Hungary, 2015, pp. 1–4, **DOI**: 10.1109/ICTON.2015.7193445.

[14] Papoulis, A. "The Fourier Integral and Its Applications." New York: McGraw-Hill, pp. 244–245 and 252–253, 1962.

[15] Donát Takács, Boldizsár Markotics and Levente Dudás," Processing and Visualizing the Low Earth Orbit Radio Frequency Spectrum Measurement Results From the SMOG Satellite Project", *Infocommunications Journal*, Vol. XIII, No 1, March 2021, pp. 18–25.

[16] Yasir Ahmed Idris Humad, and Levente Dudás, "Wide Band Spectrum Monitoring System from 30MHz to 1800MHz with limited Size, Weight and Power Consumption by MRC-100 Satellite2, *Infocommunications Journal*, Vol. XIV, No 2, June 2022, pp. 56–63.,
DOI: 10.36244/ICJ.2022.2.6

[17] Homepage of predict. https://www.qsl.net/kd2bd/predict.html Accessed October 25, 2023.

Tibor Herman received his electrical engineering BSc and MSc degree from Budapest University of Technology and Economics in 2014 and 2016 respectively. He is currently a PhD student at the Department of Broadband Infocommunications an Electromagnetic Theory. His research area focuses on Small Satellite Subsystems, involving PocketQubes developed by students and lecturers of the department, radio communication hardware development and antenna design.

Levente Dudás received his electrical engineering MSc degree in 2007 and his PhD in 2018 at Budapest University of Technology and Economics. His research topic is Radar and Satellite Applications of Radio and Antenna Systems. He is currently a senior lecturer at the Department of Broadband Infocommunications an Electromagnetic Theory, working in the Radar and Remote Sensing Laboratory. His fields of interest are active and passive radar, CubeSat and PocketQube satellite development, analog high frequency hardware and antenna design, automated and remote controlled satellite tracking and signal processing.